

Theory of electronic states and optical absorption in carbon nanotubes

Tsuneya ANDO

Department of Physics, Tokyo Institute of Technology
2-12-1 Ookayama, Meguro-ku, Tokyo 152-8551, Japan

ABSTRACT

A brief review is given of electronic and optical properties of carbon nanotubes mainly from a theoretical point of view. The topics cover an effective-mass description of electronic states, Aharonov-Bohm effects, and optical absorption including interaction effects on the band structure gap and excitonic effects.

Keywords: graphite, effective-mass approximation, exciton, Aharonov-Bohm effect, band-gap renormalization

1. INTRODUCTION

Carbon nanotubes (CNs) are quasi-one-dimensional materials made of sp^2 -hybridized carbon networks¹ and have been a subject of an extensive study. In particular, the electronic structure of a single CN has been studied theoretically, which predicted that CN becomes either metallic or semiconducting depending on its chiral vector, i.e., boundary conditions in the circumference direction.²⁻¹¹ These predictions have been confirmed by Raman experiments¹² and direct measurements of local density of states by scanning tunneling spectroscopy.¹³⁻¹⁵ The purpose of this paper is to give a brief review of recent theoretical study on electronic and optical properties of carbon nanotubes.

In understanding electronic properties of nanotubes, a $\mathbf{k}\cdot\mathbf{p}$ method or an effective-mass approximation¹¹ is quite powerful. It has been used successfully in the study of wide varieties of electronic properties of CN. Some of such examples are magnetic properties¹⁶ including the Aharonov-Bohm effect on the band gap, optical absorption spectra,¹⁷ exciton effects,¹⁸ lattice instabilities in the absence^{19,20} and presence of a magnetic field,²¹ magnetic properties of ensembles of nanotubes,²² effects of spin-orbit interaction,²³ effects of lattice vacancies,^{24,25} and electronic properties of nanotube caps.²⁶ Long wavelength phonons and electron-phonon scattering have also been studied.²⁷ In this paper, we shall discuss electronic states and optical spectra obtained mainly in this $\mathbf{k}\cdot\mathbf{p}$ scheme.

2. ENERGY BANDS

2.1. Neutrino on cylinder surface

Figure 1 shows the lattice structure and the first Brillouin zone of a two-dimensional (2D) graphite together with the coordinate systems. A unit cell contains two carbon atoms denoted by A and B. A nanotube is specified by a chiral vector $\mathbf{L} = n_a\mathbf{a} + n_b\mathbf{b}$ with integer n_a and n_b and basis vectors \mathbf{a} and \mathbf{b} ($|\mathbf{a}| = |\mathbf{b}| = a = 2.46 \text{ \AA}$). In the coordinate system fixed onto the graphite sheet, we have $\mathbf{a} = (a, 0)$ and $\mathbf{b} = (-a/2, \sqrt{3}a/2)$. For convenience we introduce another coordinate system where the x direction is along the circumference \mathbf{L} and the y direction is along the axis of CN. The direction of \mathbf{L} is denoted by the chiral angle η . It should be noted that there is another convention of choosing the basis vectors \mathbf{a}_1 and \mathbf{a}_2 instead of \mathbf{a} and \mathbf{b} such that $\mathbf{a}_1 = \mathbf{a} + \mathbf{b}$ and $\mathbf{a}_2 = \mathbf{b}$.

A graphite sheet is a zero-gap semiconductor in the sense that the conduction and valence bands consisting of π states cross at K and K' points of the Brillouin zone, whose wave vectors are given by $\mathbf{K} = (2\pi/a)(1/3, 1/\sqrt{3})$ and $\mathbf{K}' = (2\pi/a)(2/3, 0)$.^{28,29} Electronic states near a K point of 2D graphite are described by the $\mathbf{k}\cdot\mathbf{p}$ equation:^{11,30}

$$\gamma(\vec{\sigma} \cdot \hat{\mathbf{k}})\mathbf{F}(\mathbf{r}) = \varepsilon\mathbf{F}(\mathbf{r}), \quad \mathbf{F}(\mathbf{r}) = \begin{pmatrix} F_A(\mathbf{r}) \\ F_B(\mathbf{r}) \end{pmatrix}, \quad (1)$$

E-mail: ando@phys.titech.ac.jp URL: <http://www.stat.phys.titech/ando/>

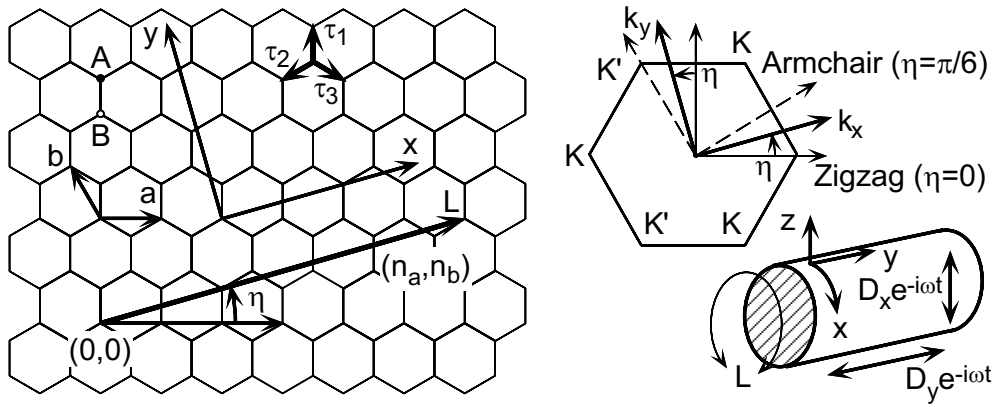


Figure 1. Left: Lattice structure of two-dimensional graphite sheet. η is the chiral angle. The coordinates are chosen in such a way that x is along the circumference of a nanotube and y is along the axis. Right-top: The first Brillouin zone and K and K' points. Right-bottom: The coordinates for a nanotube.

where γ is the band parameter, $\hat{\mathbf{k}} = (\hat{k}_x, \hat{k}_y)$ is a wave-vector operator, ε is the energy, and σ_x and σ_y are the Pauli spin matrices. Equation (1) has the form of Weyl's equation for neutrinos, i.e., relativistic Dirac electrons with vanishing rest mass. Figure 2 shows the energy dispersion and the density of states schematically.

The electronic states in a nanotube can be obtained by imposing the periodic boundary condition in the circumference direction $\Psi(\mathbf{r}+\mathbf{L})=\Psi(\mathbf{r})$ except for extremely thin CNs. The Bloch functions at a K point change their phase by $\exp(i\mathbf{K}\cdot\mathbf{L}) = \exp(2\pi i\nu/3)$, where ν is an integer defined by $n_a + n_b = 3M + \nu$ with integer M and can take 0 and ± 1 . Because $\Psi(\mathbf{r})$ is written as a product of the Bloch function and the envelope function, i.e., the neutrino wave function, this phase change should be canceled by that of the envelope functions and the boundary conditions become $\mathbf{F}(\mathbf{r}+\mathbf{L}) = \mathbf{F}(\mathbf{r}) \exp(-2\pi i\nu/3)$. The extra phase can be regarded as a fictitious Aharonov-Bohm flux passing through the cross section of CN.

Energy levels in CN for the K point are obtained by putting $k_x = \kappa_\nu(n)$ with $\kappa_\nu(n) = (2\pi/L)[n - (\nu/3)]$ and $k_y = k$ in the above $\mathbf{k}\cdot\mathbf{p}$ equation as $\varepsilon_\nu^{(\pm)}(n, k) = \pm\gamma\sqrt{\kappa_\nu(n)^2 + k^2}$,¹¹ where $L = |\mathbf{L}|$, n is an integer, and the upper (+) and lower (-) signs represent the conduction and valence bands, respectively. The Hamiltonian and the boundary condition for the K' point are obtained by replacing \hat{k}_y by $-\hat{k}_y$ and ν by $-\nu$. This shows that CN becomes metallic for $\nu=0$ and semiconducting with gap $E_g = 4\pi\gamma/3L$ for $\nu = \pm 1$. Figure 3 shows a schematic illustration of the bands for $\nu=0$ and $+1$ in the vicinity of the K point.

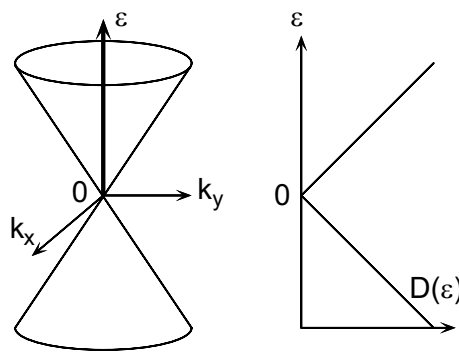


Figure 2. The energy dispersion and density of states in the vicinity of K and K' points obtained in a $\mathbf{k}\cdot\mathbf{p}$ scheme

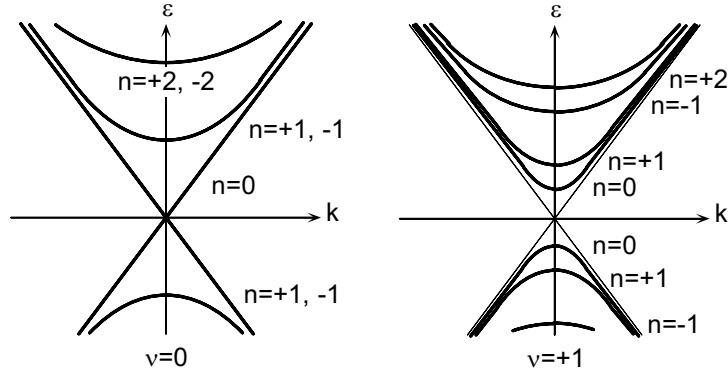


Figure 3. Energy bands of a nanotube obtained in the effective-mass approximation for $\nu=0$ (left) and $\nu=+1$ (right)

2.2. Aharonov-Bohm effect

In the presence of a magnetic flux ϕ passing through the cross section of CN, the boundary condition changes into $\Psi(\mathbf{r}+\mathbf{L}) = \Psi(\mathbf{r}) \exp(2\pi i\varphi)$ with $\varphi = \phi/\phi_0$, where $\phi_0 = ch/e$ is the magnetic flux quantum. Consequently, $\kappa_\nu(n)$ is replaced by $\kappa_{\nu\varphi}(n)$ with

$$\kappa_{\nu\varphi}(n) = \frac{2\pi}{L} \left(n + \varphi - \frac{\nu}{3} \right). \quad (2)$$

The corresponding result for the K' point is again obtained by the replacement $\nu \rightarrow -\nu$. The band gap exhibits an oscillation between 0 and $2\pi\gamma/L$ with period ϕ_0 as is shown in Fig. 4.^{11,31} This giant Aharonov-Bohm (AB) effect on the band gap is a unique property of CN's. The AB effect appears also in a tunneling conductance across a finite-length CN.³²

This AB effect was shown to be responsible for observed oscillation of the resistance in multi-wall nanotubes.³³ Quite recently, splitting of the band gap in semiconducting tubes in the presence of magnetic flux was observed directly in optical absorption spectra of single-wall CN's.³⁴

2.3. Topological singularity and absence of backward scattering

The wave function in the 2D graphite is written explicitly as

$$\mathbf{F}_{s\mathbf{k}} = \frac{1}{\sqrt{2}} \begin{pmatrix} e^{i\theta(\mathbf{k})} \\ s \end{pmatrix} \exp(i\mathbf{k}\cdot\mathbf{r}), \quad (3)$$

where $\theta(\mathbf{k})$ is the direction angle of \mathbf{k} and $s = +1$ and -1 for the conduction and valence band, respectively. This wave function acquires Berry's phase $-\pi$ when the wave vector \mathbf{k} is rotated around the origin $\mathbf{k} = 0$, although it looks continuous as a function of \mathbf{k} .^{35,36} In fact, when \mathbf{k} is rotated once in the anticlockwise direction adiabatically as a function of time t for a time interval $0 < t < T$ with $\mathbf{k}(T) = \mathbf{k}(0)$, the wavefunction $\mathbf{F}_{s\mathbf{k}}$ is changed into $\mathbf{F}_{s\mathbf{k}} \exp(-i\psi)$, where ψ is Berry's phase given by

$$\psi = -i \int_0^T dt \left\langle s\mathbf{k}(t) \left| \frac{d}{dt} \right| s\mathbf{k}(t) \right\rangle = -\pi. \quad (4)$$

This is equivalent to the well-known signature change of the spinor wave function or a spin rotation operator under a 2π rotation.

It should be noted that $\psi = -\pi$ when the closed contour encircles the origin $\mathbf{k} = 0$ but $\psi = 0$ when the contour does not contain $\mathbf{k} = 0$. Further, the wave function at $\mathbf{k} = 0$ depends on the direction of \mathbf{k} and its "spin" direction is undefined. These facts show the presence of a topological singularity at $\mathbf{k} = 0$. The nontrivial Berry's phase leads to the unique property of a metallic carbon nanotube that there exists no backscattering and the tube is a perfect conductor even in the presence of scatterers.^{35,37} In fact, it has been proved that the Born series for

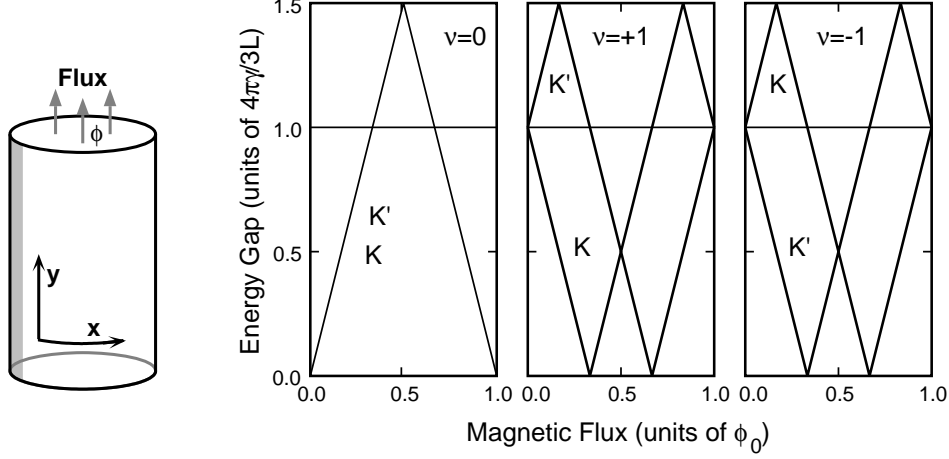


Figure 4. A schematic illustration of magnetic flux passing through a tube cross section (left) and energy gap versus the flux for metallic ($\nu=0$) and semiconducting ($\nu=\pm 1$) CN (right).

backscattering vanish identically and the conductance calculated exactly for finite-length nanotubes containing many impurities has shown to be given by $2e^2/\pi\hbar$ independent of length.³⁷ The absence of backscattering has been confirmed also by numerical calculations in a tight binding model.³⁸

Backscattering corresponds to a rotation of the \mathbf{k} direction by $\pm\pi$. In the absence of a magnetic field, there exists a time reversal process corresponding to each backscattering. This process corresponds to a rotation by $\pm\pi$ in the opposite direction. The scattering amplitudes of these two processes are same in the absolute value but have opposite signatures because of Berry's phase. As a result, the backscattering amplitude cancels out completely. In semiconducting nanotubes, on the other hand, backscattering appears because the symmetry is destroyed by a nonzero Aharonov-Bohm magnetic flux. The singularity causes also the appearance of a perfectly conducting channel and makes the conductivity infinite even in the presence of several bands at the Fermi level.³⁹ It gives rise to various zero-mode anomalies in transport properties of 2D graphite.^{40, 41}

3. OPTICAL ABSORPTION, BAND GAPS, AND EXCITONS

3.1. Polarization and selection rules

The optical absorption is described by a dynamical conductivity obtained in a linear response theory.¹⁷ We first expand electric field $E_\alpha(\theta, \omega)$ and induced current density $j_\alpha(\theta, \omega)$ into a Fourier series:

$$E_\alpha(\theta, \omega) = \sum_l E_\alpha^l(\omega) \exp(il\theta - i\omega t), \quad j_\alpha(\theta, \omega) = \sum_l j_\alpha^l(\omega) \exp(il\theta - i\omega t), \quad (5)$$

with $\alpha = x, y$ and $\theta = 2\pi x/L$. It is quite straightforward to show that the induced current has the same Fourier component as that of the electric field, i.e., $j_\alpha^l(\omega) = \sigma_{\alpha\alpha}^l(\omega) E_\alpha^l(\omega)$. The dynamical conductivity is given by

$$\sigma_{\alpha\alpha}^l(\omega) = \sum_{nk} \frac{|(n, k, +|j_\alpha^l|n+l, k, -)|^2}{iLA[\varepsilon_n^{(+)}(k) - \varepsilon_{n+l}^{(-)}(k)]} \frac{f[\varepsilon_{n+l}^{(-)}(k)](1 - f[\varepsilon_n^{(+)}(k)])2\hbar^2\omega}{[\varepsilon_n^{(+)}(k) - \varepsilon_{n+l}^{(-)}(k)]^2 - (\hbar\omega)^2 - i\hbar^2\omega/\tau}, \quad (6)$$

where A is the length of the nanotube, the current-density operator is given by $j_\alpha^l = -(e\gamma/\hbar)\sigma_\alpha e^{-il\theta}$, a phenomenological relaxation time τ has been introduced, and $f(\varepsilon)$ is the Fermi distribution function.

When external electric field \mathbf{D} is polarized along the CN axis, the Fourier components of a total field are $E_y^l = D_y\delta_{l,0}$ and the absorption is proportional to $\text{Re}\sigma_{yy}(\omega)$ with $\sigma_{yy}(\omega) = \sigma_{yy}^{l=0}(\omega)$. It can be seen from Eq. (6) that transitions occur between valence and conduction bands with the same band index n . At a band edge

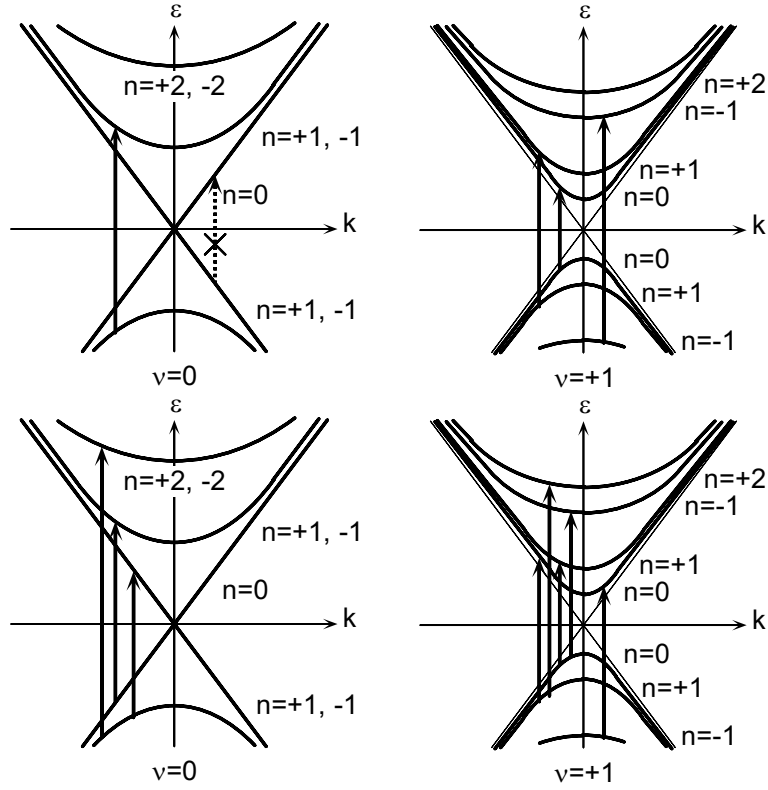


Figure 5. The band structures of a metallic and semiconducting CN. The allowed optical transitions for the parallel polarization are denoted by arrows in the upper figure and those for the perpendicular polarization in the lower figure.

$k=0$, in particular, the envelope function is given by an eigenvector of a Pauli matrix σ_x . Because the current operator j_y is proportional to σ_y , the transitions at their edges are all allowed.

The situation becomes much more complicated when an external electric field is polarized in the direction perpendicular to the CN axis. In this case, effects of an electric field induced by the polarization of nanotubes should be considered. This depolarization effect can be calculated also in the $\mathbf{k}\cdot\mathbf{p}$ scheme.

Suppose an external electric field $D_x^l e^{i\theta - i\omega t}$ is applied in the direction normal to the tube axis and let j_x^l be the induced current. Then, the corresponding induced charge density localized on the cylindrical surface is calculated as $\rho^l = (2\pi/L)(l/\omega)j_x^l$ with the use of the equation of continuity. This charge leads to potential $\phi^l = (L/\kappa|l|)\rho^l$ or electric field $E_x^l = -i(2\pi/\kappa L)l\phi^l$. The static dielectric constant κ describes polarization of states (σ and π bands) except those lying in the vicinity of the Fermi level. It is expected to be in the range $1 < \kappa < 10$, but its exact value is not known. Thus, the total electric field becomes $E_x^l = D_x^l - i|l|(4\pi^2/\kappa L\omega)j_x^l$, which leads with the use of $j_x^l = \sigma_{xx}^l E_x^l$ to $j_x^l = \tilde{\sigma}_{xx}^l D_x^l$, where

$$\tilde{\sigma}_{xx}^l = \sigma_{xx}^l \left(1 + i|l| \frac{4\pi^2}{\kappa L\omega} \sigma_{xx}^l \right)^{-1}. \quad (7)$$

For the light-polarization perpendicular to the tube axis, its field is written as $\mathbf{D} = (D_x \sin \theta, 0)$. The absorption in a unit area is then proportional to $\text{Re}(j_x E_x^*) \propto \text{Re} \tilde{\sigma}_{xx}(\omega)$ with $\tilde{\sigma}_{xx} = \tilde{\sigma}_{xx}^{l=1} = \tilde{\sigma}_{xx}^{l=-1}$. According to Eq. (6) the absorption occurs between the valence band with index n and the conduction bands with $n \pm 1$.

Let us consider a spectral edge corresponding to $k=0$, for which the eigenstates are those of a Pauli matrix σ_x . Because the current operator is proportional to σ_x , transitions between valence- and conduction-band states become allowed only when $\kappa_{\nu\varphi}(n)$ and $\kappa_{\nu\varphi}(n \pm 1)$ have a sign opposite to each other. This leads to the conclusion

in a metallic CN, for example, that transitions from $n=0$ to $n=-1$ and from $n=-1$ to $n=0$ are allowed as shown in Fig. 5. When the depolarization effect is included, however, these peaks disappear almost completely because most of their intensity is transferred to interband plasmons with much higher energy.¹⁷ Therefore, interband optical transitions among valence and conduction bands near the Fermi level is observable only for polarization parallel to the tube axis.

3.2. Band gap renormalization and excitons

One important problem is a many-body effect on the band structure and optical absorption spectrum. In fact, band gaps are likely to be influenced strongly by electron-electron interactions. Further, the exciton binding energy becomes infinite in the limit of an ideal one-dimensional electron-hole system.^{42,43} This means that the exciton effect can be quite important and modify the absorption spectra drastically. The band-gap renormalization and optical spectra with exciton effects have been calculated in the conventional screened Hartree-Fock approximation within a $\mathbf{k}\cdot\mathbf{p}$ scheme.¹⁸

The strength of the Coulomb interaction is specified by $(e^2/\kappa L)/(2\pi\gamma/L)$, which turns out to be independent of the circumference length L . In the $\mathbf{k}\cdot\mathbf{p}$ scheme, therefore, all physical quantities become almost universal if the length is scaled by L and the energy by $2\pi\gamma/L$. This parameter is estimated as $(e^2/\kappa L)(2\pi\gamma/L)^{-1} = 0.3545 \times \kappa^{-1}$ for $\gamma = 6.46 \text{ eV}\cdot\text{\AA}$, which corresponds to $\gamma = \sqrt{3}a|\gamma_0|/2$ with $\gamma_0 = -3.03 \text{ eV}$ and $a = 2.46 \text{ \AA}$.

Figure 6 shows some examples of calculated exciton energy levels for a semiconducting CN ($\nu=1$) versus the strength of the Coulomb interaction in the left hand side. With the increase of the interaction, the number of exciton bound states increases and their energy levels are shifted to the higher energy side in spite of the fact that their binding energy increases. The reason is in the considerable enhancement of the band gap due to the Coulomb interaction. It is interesting to notice that the energy of the lowest excitonic state varies very little as a function of the strength of the Coulomb interaction.

Figure 6 shows calculated absorption spectra in a semiconducting CN for $(e^2/\kappa L)/(2\pi\gamma/L) = 0.1$ in the right hand side. The energy levels of excitons are denoted by vertical straight lines. The considerable optical intensity is transferred to the lowest exciton bound states. For a sufficiently larger strength of the Coulomb interaction, transitions to exciton excited states become appreciable.

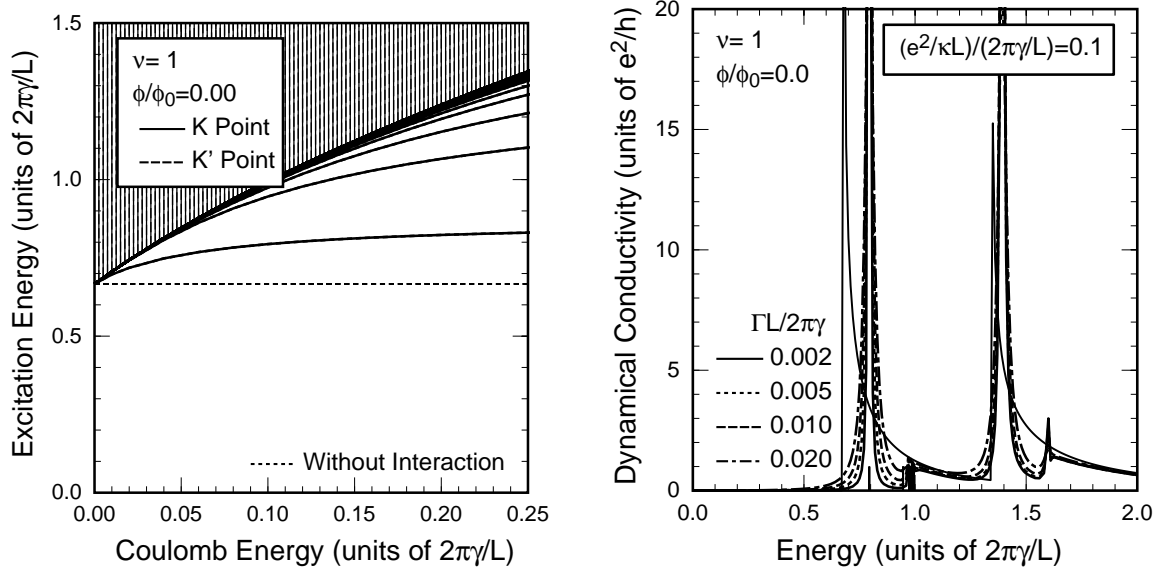


Figure 6. Interband excitation spectra calculated in a screened Hartree-Fock approximation (left) and examples of interband optical absorption spectra in the presence of electron-electron interaction (right).

In addition to excitons associated with the highest valence and the lowest conduction bands ($n=0$), exciton effects are important for transitions to excited bands. In fact, the exciton binding energy and the intensity transfer is larger for the transition to the higher conduction band ($n=1$) than those with $n=0$. This arises because the effective mass along the axis direction for the conduction and valence bands with $n=1$ is twice as large as that of the lowest conduction band and the highest valence band with $n=0$.

It turned out that interaction effects on the band gap are almost independent of $n=0$ and $n=1$ and the exciton energy is almost as large as the band-gap renormalization for the bands with larger optical gap $n=1$. As a result, the absorption peak stays almost at the corresponding band gap in the absence of interaction for $n=1$ and exciton effects independent of the interaction strength and the energy difference between the absorption peaks for $n=0$ and $n=1$ becomes smaller than that in the absence of interactions.

Optical absorption spectra of thin film samples of single-wall nanotubes were observed quite recently and analyzed by assuming a distribution of their chirality and diameter.⁴⁴ Careful comparison of the observed spectrum with calculated in a simple tight-binding model suggested the importance of excitonic effects.⁴⁵ In fact, comparing the observed spectrum with the calculated one in the fundamental absorption region, the observed absorption band for $n=0$ lies at an energy higher than half of the band for $n=1$. The results can roughly be explained by the theoretical result for $(e^2/\kappa L)/(2\pi\gamma/L) \sim 0.05$. This strongly suggests that the exciton effect together with the band-gap renormalization plays an important role in the optical transition near the fundamental absorption edge in semiconducting nanotubes.

3.3. Interaction effects on band structure

In the screened Hartree-Fock approximation discussed above, a dielectric function appearing in the self-energy is replaced by the static one and therefore dynamical effects such as coupling with charge density excitations are not taken into consideration explicitly. Quite recently, calculations were performed in a full dynamical random-phase approximation (RPA),^{46,47} often called the GW approximation,⁴⁸

In RPA, the Coulomb interaction appearing in the self-energy diagram $\Sigma_{ns}(k, \varepsilon)$ is screened by the dynamical dielectric function $\varepsilon_{n-m}(q, \omega)$. The self-energy diverges logarithmically and therefore a cutoff function $g_0(\varepsilon) = \varepsilon_c^{\alpha_c} / (|\varepsilon|^{\alpha_c} + \varepsilon_c^{\alpha_c})$ is introduced so as to exclude contributions from states far away from the Fermi level. The cutoff energy ε_c is of the order of the width of the π bands in 2D graphite.

The single-particle energy $E_{ns}(k)$ is calculated by $E_{ns}(k) = \varepsilon_n^{(s)}(k) + \Sigma_{ns}(k, \varepsilon_n^{(s)}(k))$ with $s = \pm$. Originally, it is determined by the equation obtained from the above by the replacement of $\Sigma_{ns}(k, \varepsilon_n^{(s)}(k))$ by $\Sigma_{ns}(k, E_{ns}(k))$. However, the present procedure is known to give more accurate results if the self-energy is calculated only in the lowest order.^{49,50} Using the single-particle energy, we evaluate the band gap Δ_n which is defined by the energy difference at $k=0$ between conduction and valence bands of the same index n as $\Delta_n = E_{n+}(0) - E_{n-}(0)$. The cutoff parameters are chosen as $\varepsilon_c/(2\pi\gamma/L) = 5$ and $\alpha_c = 4$.

Figure 7 gives the gap of the first parabolic band in a metallic CN and the first and second band gap for a semiconducting CN. In the regime of very weak interaction $(e^2/\kappa L)/(2\pi\gamma/L) < 0.05$, the band gap increases with the interaction strength in both metallic and semiconducting CN's. With the further increase of the interaction, however, the gap in a metallic CN starts to decrease after taking a maximum at around $(e^2/\kappa L)/(2\pi\gamma/L) \approx 0.15$, while that in a semiconducting CN continues to increase.

In the weak interaction regime $(e^2/\kappa L)/(2\pi\gamma/L) < 0.2$, dynamical effects on the band gap are small and the static RPA works well. When the interaction is stronger, the difference between the dynamical and static RPA becomes larger in a metallic CN than in a semiconducting CN. The shift in the gaps of a semiconducting CN is nearly independent of the band. This shows that the interaction effects cannot be absorbed into a simple renormalization of the band parameter γ .

Figure 8 shows the band gaps for a semiconducting CN for different cutoffs, $\varepsilon_c/(2\pi\gamma/L) = 2.5, 5.0, \text{ and } 10$. The band gap scaled by $2\pi\gamma/L$ increases logarithmically with the increase of the cutoff energy. This logarithmic cutoff dependence means that the band-gap enhancement increases slightly (logarithmically) with the increase of the CN diameter if being scaled by $2\pi\gamma/L$. Unfortunately, experimental measurements of band gaps have not been accurate enough to make detailed comparison possible so far. Note that such logarithmic dependence

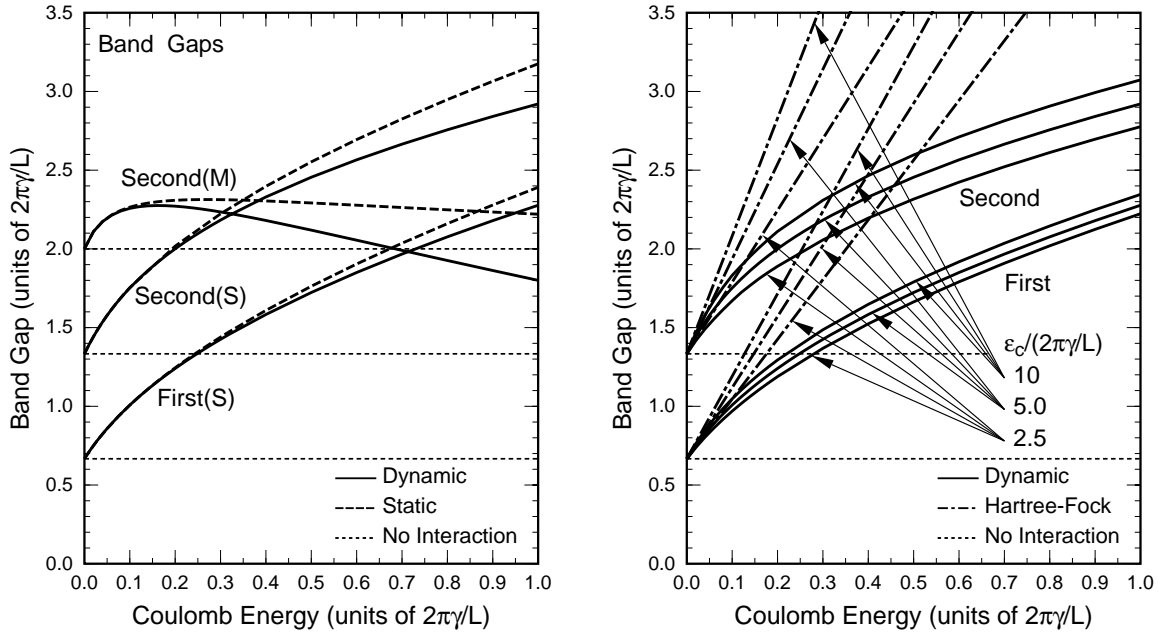


Figure 7. (Left) Calculated gap of a parabolic bands ($n = \pm 1$) in a metallic CN (M) and first and second gaps of a semiconducting CN (S) versus the effective strength of the Coulomb interaction.

Figure 8. (Right) The cutoff-energy dependence of the gap in a semiconducting nanotube. The gap increases logarithmically with the thickness after being scaled by $2\pi\gamma/L$.

on the diameter cannot be reproduced in the conventional local-density approximation used in first-principles calculations.

If we employ the same scheme, we can calculate the self-energy for the linear bands with $n = 0$ in metallic CN's, giving a gapless linear band with a renormalized velocity. In fact, although each term of perturbation expansion of the self-energy is known to exhibit a divergence, the RPA self-energy itself does not diverge because of the cancellation of a divergent polarization function. This result is in clear contradiction with the fact that only a charge-density and a spin-density excitation can exist and there are no well-defined quasi-particle excitations in systems with a linear dispersion,^{51,52} leading to the breakdown of the Fermi liquid picture.

This apparent inconsistency arises from the way of determining the quasi-particle energy from the self-energy. Even in RPA, the spectral function (the imaginary part of the Green's function) exhibits double sharp peaks in a system with only metallic linear bands as shown in Fig. 9. This peak splitting, into charge-density and spin-density excitations presumably, is a result of the divergent behavior of the polarization function and qualitatively in agreement with that of the spectral function for a Tomonaga-Luttinger liquid reported in refs. 53 and 54. For the parabolic bands both in semiconducting and metallic CN's, no singular behavior appears in the polarization function and therefore quasi-particle states are expected to give a good picture of their low-energy excitations.

4. SUMMARY AND CONCLUSION

In summary, an electron in a nanotube is a massless neutrino on a cylinder surface with a fictitious Aharonov-Bohm flux determined by its structure. A nanotube becomes a metal or a semiconductor, depending on whether the amount of the flux vanishes or not. In the presence of an external magnetic flux, the band structure changes due to a large Aharonov-Bohm effect. One important feature of the neutrino equation is the presence of a topological singularity at the origin of the wave-vector space, leading to the absence of backward scattering and the presence of a perfectly conducting channel even in the presence of scatterers.

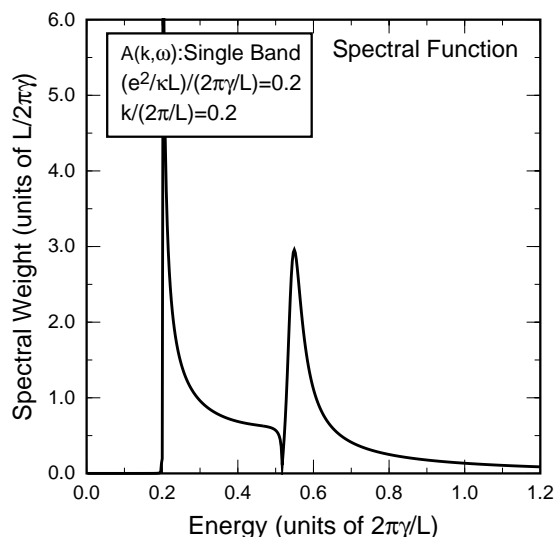


Figure 9. An example of the spectral function in a single linear-band model calculated in RPA. The energy of the first peak corresponds well to the spin-density excitation and the second to the charge-density excitation.

Optical absorptions are appreciable only for polarization parallel to the axis. Because of the dimensionality of a nanotube, excitonic effects are expected to play important roles in optical spectra. Explicit calculations of the band structure with the inclusion of effects of electron-electron interactions in several approximation schemes demonstrate a considerable band-gap enhancement depending on the strength of a dimensionless interaction parameter. Calculations of optical excitation spectra show that excitonic effects can also be important.

ACKNOWLEDGMENTS

This work was supported in part by a 21st Century COE Program at Tokyo Tech “Nanometer-Scale Quantum Physics” and by Grants-in-Aid for Scientific Research and for COE (12CE2004 “Control of Electrons by Quantum Dot Structures and Its Application to Advanced Electronics”) from Ministry of Education, Culture, Sports, Science and Technology Japan. Numerical calculations were performed in part using the facilities of the Supercomputer Center, Institute for Solid State Physics, University of Tokyo.

REFERENCES

1. S. Iijima, *Nature (London)* **354**, 56 (1991).
2. N. Hamada, S. Sawada, and A. Oshiyama, *Phys. Rev. Lett.* **68**, 1579 (1992).
3. J. W. Mintmire, B. I. Dunlap, and C. T. White, *Phys. Rev. Lett.* **68**, 631 (1992).
4. R. Saito, M. Fujita, G. Dresselhaus, and M. S. Dresselhaus, *Phys. Rev. B* **46**, 1804 (1992); *Appl. Phys. Lett.* **60**, 2204 (1992).
5. M. S. Dresselhaus, G. Dresselhaus, and R. Saito, *Phys. Rev. B* **45**, 6234 (1992).
6. R. A. Jishi, M. S. Dresselhaus, and G. Dresselhaus, *Phys. Rev. B* **47**, 16671 (1993).
7. K. Tanaka, K. Okahara, M. Okada and T. Yamabe, *Chem. Phys. Lett.* **191**, 469 (1992).
8. Y. D. Gao and W. C. Herndon, *Mol. Phys.* **77**, 585 (1992).
9. D. H. Robertson, D. W. Brenner, and J. W. Mintmire, *Phys. Rev. B* **45**, 12592 (1992).
10. C. T. White, D. C. Robertson, and J. W. Mintmire, *Phys. Rev. B* **47**, 5485 (1993).
11. H. Ajiki and T. Ando, *J. Phys. Soc. Jpn.* **62**, 1255 (1993).
12. A. M. Rao, E. Richter, S. Bandow, B. Chase, P. C. Eklund, K. W. Williams, M. Menon, K. R. Subbaswamy, A. Thess, R. E. Smalley, G. Dresselhaus, and M. S. Dresselhaus, *Science* **275**, 187 (1997).

13. C. H. Olk and J. P. Heremans, *J. Mater. Res.* **9**, 259 (1994).
14. J. W. Wildoer, L. C. Venema, A. G. Rinzier, R. E. Smalley, and C. Dekker, *Nature (London)* **391**, 59 (1998).
15. A. Hassanien, M. Tokumoto, Y. Kumazawa, H. Kataura, Y. Maniwa, S. Suzuki, and Y. Achiba, *Appl. Phys. Lett.* **73**, 3839 (1998).
16. H. Ajiki and T. Ando, *J. Phys. Soc. Jpn.* **62**, 2470 (1993). [Errata, *J. Phys. Soc. Jpn.* **63**, 4267 (1994).]
17. H. Ajiki and T. Ando, *Physica B* **201**, 349 (1994); *Jpn. J. Appl. Phys. Suppl.* **34-1**, 107 (1995).
18. T. Ando, *J. Phys. Soc. Jpn.* **66**, 1066 (1997).
19. N. A. Viet, H. Ajiki, and T. Ando, *J. Phys. Soc. Jpn.* **63**, 3036 (1994).
20. H. Suzuura and T. Ando, *Proceedings of 25th International Conference on the Physics of Semiconductors*, edited by N. Miura and T. Ando (Springer, Berlin, 2001), p. 1525.
21. H. Ajiki and T. Ando, *J. Phys. Soc. Jpn.* **64**, 260 (1995); **65**, 2976 (1996).
22. H. Ajiki and T. Ando, *J. Phys. Soc. Jpn.* **64**, 4382 (1995).
23. T. Ando, *J. Phys. Soc. Jpn.* **69**, 1757 (2000).
24. T. Ando, T. Nakanishi, and M. Igami, *J. Phys. Soc. Jpn.* **68**, 3994 (1999).
25. M. Igami, T. Nakanishi, and T. Ando, *J. Phys. Soc. Jpn.* **70**, 481 (2001).
26. T. Yaguchi and T. Ando, *J. Phys. Soc. Jpn.* **70**, 3641 (2001); *ibid* **71**, 2224 (2002).
27. H. Suzuura and T. Ando, *Physica E* **6**, 864 (2000); *Mol. Cryst. Liq. Cryst.* **340**, 731 (2000); *Phys. Rev. B* **65**, 235412 (2002).
28. P. R. Wallace, *Phys. Rev.* **71**, 622 (1947).
29. G. S. Painter and D. E. Ellis, *Phys. Rev. B* **1**, 4747 (1970).
30. J. C. Slonczewski and P. R. Weiss, *Phys. Rev.* **109**, 272 (1958).
31. J. P. Lu, *Phys. Rev. Lett.* **74**, 1123 (1995).
32. W. -D. Tian and S. Datta, *Phys. Rev. B* **49**, 5097 (1994).
33. A. Fujiwara, K. Tomiyama, H. Suematsu, M. Yumura, and K. Uchida, *Phys. Rev. B* **60**, 13492 (1999).
34. S. Zaric, G. N. Ostojic, J. Kono, X. Wei, M. S. Strano, V. C. Moore, R. H. Hauge, and R. E. Smalley, *Proceedings of 6th International Symposium on New Phenomena in Mesoscopic Structures, Maui, USA, 2003* (in press).
35. T. Ando, T. Nakanishi, and R. Saito, *J. Phys. Soc. Jpn.* **67**, 2857 (1998).
36. M. V. Berry, *Proc. Roy. Soc. London* **A392**, 45 (1984).
37. T. Ando and T. Nakanishi, *J. Phys. Soc. Jpn.* **67**, 1704 (1998).
38. T. Nakanishi and T. Ando, *J. Phys. Soc. Jpn.* **68**, 561 (1999).
39. T. Ando and H. Suzuura, *J. Phys. Soc. Jpn.* **71**, 2753 (2002).
40. N. H. Shon and T. Ando, *J. Phys. Soc. Jpn.* **67**, 2421 (1998).
41. T. Ando, Y. Zheng, and H. Suzuura, *J. Phys. Soc. Jpn.* **71**, 1318 (2002).
42. R. Loudon, *Am. J. Phys.* **27**, 649 (1959).
43. R. J. Elliot and R. Loudon, *J. Phys. Chem. Solids* **8**, 382 (1959); **15**, 196 (1960).
44. H. Kataura, Y. Kumazawa, Y. Maniwa, I. Umezumi, S. Suzuki, Y. Ohtsuka and Y. Achiba, *Synth. Met.* **103**, 2555 (1999).
45. M. Ichida, S. Mizuno, Y. Tani, Y. Saito, and A. Nakamura, *J. Phys. Soc. Jpn.* **68**, 3131 (1999).
46. H. Sakai, H. Suzuura, and T. Ando, *J. Phys. Soc. Jpn.* **72**, 1698 (2003).
47. H. Sakai, H. Suzuura, and T. Ando, *Physica E* (in press).
48. L. Hedin, *Phys. Rev.* **139**, A796 (1965); A. W. Overhauser, *Phys. Rev. B* **3**, 1888 (1971); L. Hedin and S. Lundqvist, *Solid State Physics*, ed. F. Seitz, D. Turnbull and H. Ehrenreich (Academic, New York, 1969) Vol. 23, p. 1.
49. T. M. Rice, *Ann. Phys. (N.Y.)* **31**, 100 (1965).
50. D. F. Du Bois, *Ann. Phys. (N.Y.)* **7**, 174 (1959).
51. S. Tomonaga, *Prog. Theor. Phys.* **5**, 544 (1950).
52. J. M. Luttinger, *J. Math. Phys.* **4**, 1154 (1963).
53. J. Voit, *Phys. Rev. B* **47**, 6740 (1993).
54. V. Meden and K. Schonhammer, *Phys. Rev. B* **46**, 15753 (1992).